View Article Online
View Journal

Dalton Transactions

An international journal of inorganic chemistry

Accepted Manuscript

This article can be cited before page numbers have been issued, to do this please use: A. Karimata, T. Gridneva, P. H. Patil, R. R. Fayzullin, E. Khaskin, S. Lapointe, A. Garcia-Roca and J. R. Khusnutdinova, *Dalton Trans.*, 2022, DOI: 10.1039/D2DT02180C.

ROYAL SOCIETY OF CHEMISTRY

rsc.li/dalton

View Article Online
DOI: 10.1039/D2DT02180C

ARTICLE

Ethylene binding in mono- and binuclear Cu^{I} complexes with tetradentate pyridinophane ligands

Received 00th January 20xx,
Accepted 00th January 20xx

DOI: 10.1039/x0xx00000x

Ayumu Karimata, [a] Tatiana Gridneva, [a] Pradnya H. Patil, [a] Robert R. Fayzullin, [b] Eugene Khaskin, [a] Sébastien Lapointe, [a] Alèria Garcia-Roca [a] and Julia R. Khusnutdinova*[a]

Herein we report a series of Cu^{I} complexes supported by a tetradentate ^{R}N4 pyridinophane ligands that coordinate to ethylene forming either mononuclear complexes with ethylene coordinated in an η^2-mode or binuclear complexes where ethylene binds to two Cu atoms in a μ-η^2-η^2-mode, depending on sterics at the ^{R}N4 ligand and the reaction conditions. In the binuclear complex with bridging ethylene, the C=C bond is significantly elongated, with bond length of 1.444(8) Å according to X-ray diffraction analysis. This complex represents the only examine of a μ-η^2-η^2-coordinated Cu-olefin complex reported up to date, featuring one of the longest reported C=C bonds. The spectroscopic characterization, structure, electrochemical properties and solution behavior are analyzed in this study. Coordination of ethylene was found to be reversible in these complexes and more favored in less sterically hindered ^{R}N4 ligands, so that ethylene binding is observed in a coordinating solvent (MeCN) environment. In the case of the MeN4 ligand, the ethylene complex is photoluminescent in the solid state. The ethylene binding modes in mono- and binuclear compexes are elucidated through Natural Bond Orbital and QTAIM analyses.

Introduction

Ethylene, the simplest alkene, is a widely used starting material for many transition metal-catalyzed transformations in the chemical industry and it also serves as a simple plant hormone playing a role in various steps of the plant growth cycle, fruit ripening being one of the well-known examples. Ethylene was shown to bind strongly to the ETR 1 receptor in plants,[1-2] and many studies have been directed towards synthesizing simple model copper complexes that efficiently coordinate ethylene. Such complexes provide insight into the nature of ethylene binding to d^{10} metal complexes as well show potential for the development of operationally simple ethylene sensors. Since the first report of a Cu^{I}-ethylene complex supported by a tridentate tris-pyrazolylborate ligand,[3] many more examples of mononuclear Cu-ethylene complexes have been reported,[4-20] typically supported by tridentate or bidentate ligands, thus forming tetra- or tricoordinate Cu centers. Depending on the nature of the ligand, efficiency of ethylene binding varies widely, with many complexes reported to be stable only in the presence of excess ethylene, and which undergo ethylene dissociation under vacuum. Therefore, finding model complexes with high affinity to ethylene remains an important challenge, which may find application in the development of Cu-based ethylene sensors[21-23] or olefin separation methods,[24] for which reversibility of binding is also an important factor.

We have previously reported that a macrocyclic ^{R}N4 ligand forms well-defined copper complexes, in which the ^{R}N4 ligand may bind in a tetradentate or tridentate mode, depending on the nature of surrounding ligands, complex charge and steric hindrance imposed by the R-substituents of the ^{R}N4 ligand.[25-26] Some of these complexes were also shown to be photoluminescent, with PLQY highly dependent on fluxional behaviour and steric factors.[25-28] In this work, we report our studies of ethylene binding to a Cu^{I} center supported by a tetracoordinate ^{R}N4 ligand. An unusual μ-η^2-η^2 ethylene coordination was also found in the solid state, previously unreported for this metal and characterized by significant C=C bond elongation in the coordinated ethylene.

Results and discussion

Synthesis and spectroscopic properties of (RN4)Cu-ethylene complexes.

To obtain copper ethylene complexes, we selected the previously reported cationic [(^{R}N4)Cu(MeCN)]PF$_6$ complexes **1**-**3** as convenient starting materials that can be easily prepared from the common [Cu(MeCN)$_4$](PF$_6$) precursor and 1 equivalent of the ^{R}N4 ligand in acetonitrile solvent. Complexes **1** and **3** were reported previously,[25-26] while complex **2**, [(^{Me}N4)Cu(MeCN)](PF$_6$), was prepared in this work similarly to previously reported analogue [(^{Me}N4)Cu(MeCN)](BF$_4$). The ^{1}H

[a] Okinawa Institute of Science and Technology Graduate University, Coordination Chemistry and Catalysis Unit, 1919-1 Tancha, Onna-son, Okinawa, Japan, 904-0495. Email: juliak@oist.jp.
[b] Arbuzov Institute of Organic and Physical Chemistry, FRC Kazan Scientific Center, Russian Academy of Sciences, 8 Arbuzov Street, Kazan 420088, Russian Federation.

† Footnotes relating to the title and/or authors should appear here.
Electronic Supplementary Information (ESI) available: [details of any supplementary information available should be included here]. See DOI: 10.1039/x0xx00000x

View Article Online
DOI: 10.1039/D2DT02180C

and $^{13}C\{^1H\}$ NMR spectra of the isolated **2** were analogous to those of the previously characterized [(^{Me}N4)Cu(MeCN)](BF$_4$).[26] As reported previously,[25] complex **3** features reversible interconversion between two isomers showing κ^3 and κ^4 coordination modes for the ^{tBu}N4 ligand, leading to broadening of ^{1}H NMR spectra at room temperature (RT), which was resolved at low temperature showing that κ^3 and κ^4 isomers were present in a 28.5 :71.5 ratio at –5 °C in acetonitrile.[25] For less hindered **1** and **2**, the isomers with κ^4-coordinated ^{R}N4 ligand are predominant.

Exposure of acetone solutions of complexes **1**-**3** to 1 atm of ethylene led to immediate color change from orange-yellow to pale yellow, while analysis of the reaction mixtures by ^{1}H NMR showed the formation of new complexes **4**-**6** in solution (Scheme 1). The representative ^{1}H NMR spectra for complex **2** before and after exposure of ethylene are shown in Figure 1. In the presence of ethylene, methylene and aromatic peaks of the ^{Me}N4 ligand shift slightly downfield and a new singlet appears at 4.44 ppm assigned to coordinated ethylene, which is retained after the reaction mixture is evacuated and the solid residue is dissolved in acetone.

When the analogous reaction was performed in acetonitrile, competition between coordinating MeCN and ethylene led to incomplete conversion in case of complexes **1** and **2**, while no ethylene complex was formed in the more hindered complex **3** and only starting material was present (Figure S39–41).

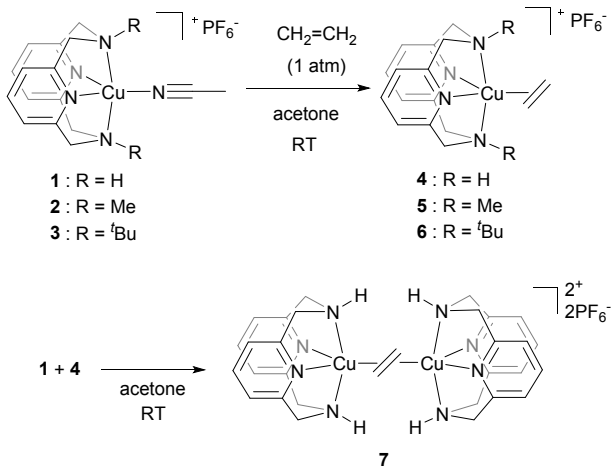

Scheme 1. Synthesis of complexes **4**-**7**.

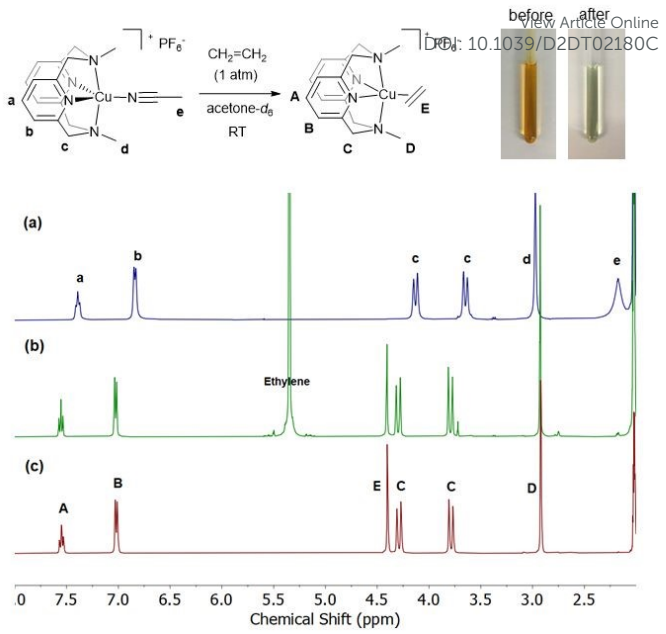

Figure 1. ^{1}H NMR spectra of **2** in acetone-d_6 at room temperature (a) before and (b) after exposure to ethylene gas, and (c) isolated **5**. Photographs above are the NMR tube before and after exposure to ethylene.

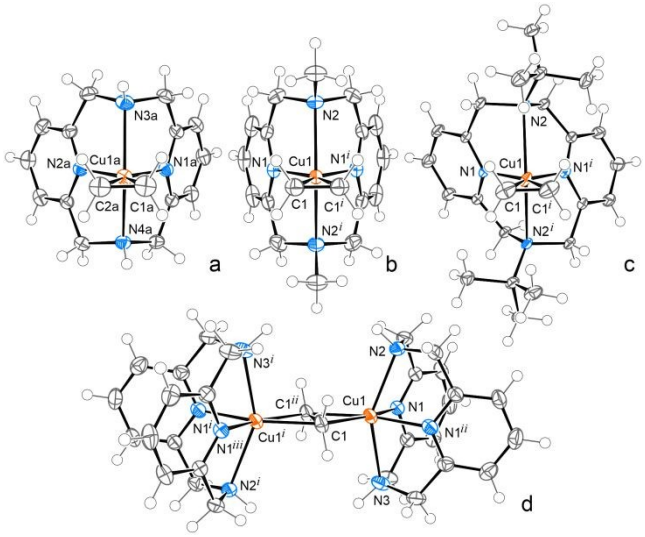

Figure 2. ORTEP of complex cations of compounds **4** (a), **5** (b), **6** (c) and **7** (d) at 60 % probability level according to SC-XRD data. For **4**, only one of two symmetry independent complexes is shown.[29]

Complexes **4**-**6** were isolated in 84-93% yields and characterized by ^{1}H and ^{13}C NMR, IR and UV-vis spectroscopy. All complexes were air-sensitive, but stable in solution or solid state under inert atmosphere of N_2 or argon even in the absence of ethylene gas or under prolonged exposure to vacuum. Single crystals were obtained by layering acetone solution of **4**-**6** with diethyl ether and the structure was determined by single crystal X-ray diffraction (SC-XRD) (Figure 2a-c). The crystals of **4** and **5** were obtained under argon atmosphere, while crystallization of **6** was conducted in the presence of excess ethylene.

Interestingly, during our initial attempts to isolate complex **4**, we found that slow evaporation of acetone solution after

View Article Online
DOI: 10.1039/D3DT02180C

exposure to ethylene led to crystallization of a binuclear complex **7**. Surprisingly, SC-XRD reveals that ethylene binds symmetrically to two (^{H}N4)Cu centers in a bridging μ-η^2-η^2 mode (Figure 2d). Alternatively, complex **7** was obtained in a more reliable way by mixing solution of mononuclear precursors **1** and **4** in acetone, from which complex **7** was isolated in a solid form by diffusion of diethyl ether vapor under nitrogen atmosphere, in the absence of added ethylene gas (Scheme 1). Poorly soluble complex **7** was not stable in solution, converting to complex **4** and insoluble precipitate and was therefore characterized only in the solid state.

The analogous reaction with more sterically hindered ^{Me}N4 and ^{tBu}N4 failed to give an analogous binuclear complexes likely due to greater steric demands imposed by substituents at the pendant amines that prevented binuclear complex formation.

The X-ray structures show that in all complexes the ^{R}N4 ligand coordinates in a κ^4-fashion, with elongated Cu–N_{amine} distances as compared to Cu–$N_{pyridine}$ (Table 1). As expected, Cu–N_{amine} distances are considerably longer for complex **6** with a bulkier ^{tBu}N4 ligand, while the shortest bonds are present in complex **4**. At the same time, Cu–$N_{pyridine}$ distances remain very similar across all studied complexes. The C=C bond distance in coordinated ethylene is longer than in free ethylene (1.34 Å),[30] with somewhat longer C=C distance (1.382(2) Å) in complex **6**.

For comparison, binuclear complex **7** features a significantly elongated C=C bond of 1.444(8) Å, along with a slightly longer Cu–C distances as compared to the mononuclear complex **4** ligated to ^{H}N4. The comparison with other reported Cu-ethylene complexes in Crystal Structure Database (CSD) shows that complex **7** features one of the longest reported C=C distances in ethylene coordinated to Cu atom. For example, the longest Cu-coordinated C=C bond in ethylene reported up to date is 1.42(3) Å,[31] although longer C=C bonds are known for Cu^{I} π-complexes with other alkenes.[32-36] Although analogous bridging coordination mode for ethylene complexes with other metals such as Zr,[37-41] Sc,[42] Hf,[38] Yb-Pt,[43] Cr,[44] Rh,[45] were reported, complex **7** represents the only example of this coordination mode for ethylene in copper complexes.

Consistent with X-ray structures, ^{1}H NMR spectra indicated that only one isomer was present in complexes **4**-**6**, representing the κ^4-coordinated ^{R}N4 ligand in acetone solution as evident from the appearance of only two doublets for the geminally coupled CH_2 groups and one set of a doublet and a triplet for pyridine groups. The ^{1}H and ^{13}C chemical shifts of coordinated ethylene for all complexes are shown in Table 2. In all cases, ^{1}H and ^{13}C chemical shifts of ethylene move upfield compared to free ethylene. The most upfield ^{13}C chemical shift for coordinated ethylene is observed for ^{tBu}N4-coordinated complex **6**, correlating with a somewhat longer C=C bond length in this complex, while δ_C in the two less hindered complexes **4** and **5** are very similar.

The comparison with the literature reported chemical shifts of the coordinated ethylene in Cu complexes (Table S2, ESI) shows that similar ^{13}C chemical shift was observed for coordinated ethylene in a β-diketiminatocopper(I) complex (δ_C 74.74; C=C 1.365(3) Å)[7] and iminophosphanamide copper(I) complex (δ_C 73.0; C=C 1.362(6) Å)[6] featuring C=C distances similar to complex **5** (δ_C 77.1; C=C 1.359(7) Å). The comparison of ^{1}H and ^{13}C NMR chemical shifts of the coordinated ethylene and the C=C bond lengths (Chart S1, Table S2 in ESI) shows that as expected, the complexes featuring significantly shorter C=C bond length are typically characterized by much more downfield shifted ^{13}C signals of coordinated ethylene, closer to the ^{13}C chemical shift of free ethylene, while the correlation with proton chemical shifts is less obvious, presumably due to greater dependence on the surrounding ligand environment.

Table 1. Selected bond distances (Å) in complexes **4**-**7** according to SC-XRD.

Complex	**4**[a]	**5**	**6**	**7**
Cu–N_{py}	2.0057(12)-2.0334(12)	2.047(3)	2.0035(8)	2.063(2)
Cu–N_{amine}	2.3454(12)-2.3858(13)	2.389(3)	2.5119(8)	2.361(4)
Cu–C	2.0039(15)-2.0251(17)	2.033(4)	2.0197(11)	2.0907(15)
C=C	1.371(2), 1.369(3)	1.359(7)	1.382(3)	1.444(8)

[a]For two independent molecules in a unit cell.

Table 2. ^{1}H and ^{13}C chemical shifts (ppm) of the coordinated ethylene in complexes **4**–**6** and free ethylene in acetone-d_6.[a]

Compound	δ_H	δ_C	$\Delta\delta_C$ [a]
4	4.32	76.8	–46.7
5	4.44	77.1	–46.4
6	4.15	75.5	–48.0
Free ethylene	5.38	123.5	0

[a]$\Delta\delta_C = \delta_{C,\,coord} - \delta_{C,\,free}$.

Considering that the previously reported (^{R}N4)Cu complexes containing halide and N-heterocyclic carbene ligands are photoluminescent,[25-28] we decided to investigate photoluminescent properties of **4**-**6** and compare them to their Cu-acetonitrile precursors. Among copper-acetonitrile complexes **1**-**3**, only most sterically hindered complex **3** showed emission with an emission peak maximum at 619 nm and a photoluminescence quantum yield (PLQY) of 0.35 in the crystal state.[25] Complexes **1** and **2** show only very weak emission, which may be attributed to the presence of more fluxional ^{R}N4 (R = H or Me) ligands, which have been shown to have a detrimental effect on emissive properties in our previous work.[26]

Surprisingly, upon coordination of ethylene, only complex **5**, with the ^{Me}N4 ligand, shows emission at 589 nm with a PLQY of 0.14 in the crystal state, while complexes **4** and **6** were not emissive in the crystal state. Complexes **5** and **6** also show photoluminescence in a rigid polymer matrix of poly(methylmethacrylate) (PMMA) (Table S1). No emission was observed in acetone solution for all complexes. Although further tuning of emission properties of these complexes is outside of the scope of this work, the formation of photoluminescent Cu-ethylene complexes may potentially lead to a promising method of the development of Cu-containing ethylene sensors, if such properties may be further optimized for observation in solution or polymer gels.

View Article Online
DOI: 10.1039/D2DT02180C

Reactivity of (^{R}N4)Cu complexes towards ethylene substitution: NMR and electrochemical investigation

Considering that all isolated complexes **4**-**6** were stable towards ethylene loss under vacuum at RT, we then set out to test their ability to retain ethylene coordination in the presence of a coordinating solvent, acetonitrile.

When isolated complexes **4**-**6** were dissolved in CD_3CN and analysed by ^{1}H NMR spectroscopy, only complex **6** showed complete displacement of ethylene by MeCN and formation of **3**. Surprisingly, even in neat CD_3CN, complexes **4** and **5** still partially retained coordinated ethylene and formed a mixture containing ethylene-bound complex as a minor component (< ca. 10-20%), free ethylene and [(^{R}N4)Cu(MeCN)](PF_6) at RT.

The addition of 93 equiv of MeCN to an acetone solution of complex **5** showed that ethylene complex **5** and acetonitrile complex **2** were present in a 20 : 21 ratio, respectively, confirming that ethylene effectively competes with MeCN for coordination at the Cu center with less sterically hindered ^{Me}N4 ligand (Figure S46). However, when 1 atm ethylene gas was reintroduced to the same reaction mixture, complex **5** immediately reformed as the only component present in the reaction mixture even in the presence of excess MeCN, showing that ethylene/MeCN substitution occurs in a reversible manner.

Another useful tool to confirm reversible ethylene binding is cyclic voltammetry, which showed a drastic change of upon ethylene displacement with MeCN. Our previous studies showed that acetonitrile complexes **1**-**3** feature chemically reversible oxidation waves with a large separation between anodic and cathodic waves, with the anodic peak potential falling in a range of –0.07 to –0.21 mV vs. Fc/Fc^+ depending on the nature of the ligand.[26] We then investigated the redox properties of complexes **4**-**6** in acetone solution in the presence of ethylene gas. Complexes **4** and **5** showed a chemically reversible oxidation wave, and complex **6** showed an irreversible oxidation peak. The anodic peak potential was found to be highly dependent on the nature of the ^{R}N4 ligand and is shifted most positively for complex **6** (Table 3). The addition of MeCN and the replacing ethylene atmosphere by purging with argon led to the appearance of characteristic, cathodically shifted peaks that corresponded to acetonitrile complexes. The representative cyclic voltammograms for complex **4** are shown in Figure 3. When 16 equiv of MeCN was added and the atmosphere was replaced with argon by purging for 5 min, the CV showed the presence of two anodic waves, one corresponding to the starting material, ethylene complex **4**, and a characteristic, more cathodically shifted peak (E_{pf} = –0.34 mV vs Fc/Fc^+), corresponding to complex **1**. When ethylene gas was reintroduced, the anodic wave for complex **1** disappeared and only the oxidation peak corresponding to **4** could be observed, showing that ethylene/acetronitrile substitution was reversible. Complex **5** showed essentially similar behaviour (Figure S49). In contrast, the ^{tBu}N4-containing complex **6** showed complete conversion to the corresponding MeCN complex **3**, which was the only species detected by CV when 16 equiv of MeCN were added under argon. The reintroduction of ethylene atmosphere led to only partial conversion back to **6**, evident from the presence of two anodic waves corresponding to **6** and **3** (Figure S50).

Overall, the results of these NMR and electrochemical studies show that in less sterically hindered complexes **4** and **5**, ethylene effectively competes even with excess MeCN, while ethylene binding is less favourable in case of more sterically demanding **6**. Ethylene coordination in these complexes leads to a significant shift of the oxidation wave towards more positive potential as compared to the analogous complexes containing a better σ-donor: the MeCN ligand.

Table 3. Electrochemical properties of complexes **1**-**6** in acetone/$^{n}Bu_4NPF_6$.[a]

Complex	E_{pf}, mV[b]	E_{pr}, mV[c]	ΔE, mV[d]	$E_{1/2}$, mV[e]
1	–0.21	–0.59	0.38	–0.40
2	–0.22	–0.41	0.19	–0.32
3	–0.07	–0.39	0.32	–0.23
4	+0.03	–0.44	0.47	–0.2
5	+0.25	–0.29	0.54	–0.02
6[f]	+0.67	n.d.	n.d.	n.d.

[a]Cyclic voltammograms for complexes **1**-**6** (1 mM) in a 0.1 M solution of $^{n}Bu_4NPF_6$ as a supporting electrolyte in acetone at 23 °C; 100 mV s^{-1} scan rate; Pt disk electrode (d = 1.6 mm); all peaks were referenced versus ferrocene. [b]Potential of the forward peak. [c]Potential of the returnpeak. [d]The peak-to-peak separation ΔE was calculated as $E_{pf} - E_{pr}$. [e]$E_{1/2}$ was estimated as $(E_{pf} + E_{pr})/2$. [f]Irreversible oxidation, no reverse peak was present. n.d. – not determined.

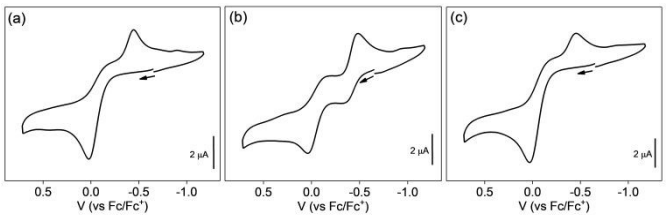

Figure 3. Cyclic voltammograms: (a) complex **4** under ethylene atmosphere; (b) complex **4** after addition of 16 equiv of MeCN under argon; and (c) same solution as (b) after replacing the atmosphere with ethylene.

Computational studies of ethylene binding in complexes 4-7.

The binding of ethylene to copper(I) is typically described through a classical Dewar-Chatt-Duncanson (DCD) model, which takes into account two major contributions to metal-olefin interactions: σ-donation from the olefin π-bonding C=C orbital to an empty orbital of a suitable symmetry at the metal and π-back-donation from a filled metal *d*-orbital to the π-antibonding C=C orbital of the olefin.[46-48] The strength of these interactions, especially π-back-donation, in turn, affects bond distances and angles around the olefinic carbons, as well as chemical shifts of the coordinated olefin in ^{13}C and ^{1}H NMR. More recently, Copéret and co-workers also reported the contribution from the ligand-to-metal donation of the olefin σ-bonding C=C orbital that were not accounted for in a classical DCD model and which were elucidated through combined computational and NMR analysis.[49]

Considering that the bridging mode of ethylene binding in the binuclear complex **7** is unusual for copper, we analysed all

View Article Online
DOI: 10.1039/D3DT02180C

complexes using a Natural Bond Orbital (NBO) approach and Quantum Theory of Atoms in Molecules (QTAIM)[50] for the DFT-optimized geometries of the cationic parts of complexes **4**-**7**. The geometry optimization was performed in the gas phase using M06L functional and SDD (for Cu)/6-31++G(d,p) (for other elements) basis set, which gave best match to experimental structures.

As expected from the DCD model, the NBO analysis of mononuclear complexes **4**-**6** shows that major contributions to ethylene binding to copper(I) are the σ-donation from predominantly π-bonding C=C orbital to a Cu-based *s*-type orbital, as well back-donation from the Cu-based $d_{x^2-y^2}$-type orbital to the π-antibonding C=C orbital of ethylene. The second order perturbation stabilization energies, $E^{(2)}$, for these interactions are summarized in Table 4, and Natural Atomic Orbital (NAO) contributions and orbital plots for all complexes are given in the ESI. NBO analysis of complex **6** shows slightly stronger π-backdonation ($E^{(2)}$ = 29.90 kcal mol^{-1}) as compared to **4** ($E^{(2)}$ = 27.82 kcal mol^{-1}) and **5** ($E^{(2)}$ = 27.74 kcal mol^{-1}), consistent with a somewhat longer C–C bond distance of the coordinated ethylene in **6**. The contribution from the donation of the σ-bonding C=C orbital to the Cu(*s*)-based orbital is very weak, essentially negligible in mononuclear complexes **4**-**6** ($E^{(2)}$ = 0.85-1.17 kcal mol^{-1}).

Similarly, the NBO analysis of the selected literature-reported Cu-ethylene complexes with N-donor ligands shows that two major contributions correspond to the expected σ-donation from π-(C=C) to Cu(*s*) and back-donation from Cu($d_{x^2-y^2}$) to the π*-(C=C) orbital of ethylene (Table S22, ESI). Stronger π(C=C)→ Cu(s) donation is observed in complexes with bidentate N-donor ligands such as 2,2'-bipyridine ($E^{(2)}$ = 91.37 kcal mol^{-1}), 1,10-phenanthroline ($E^{(2)}$ = 89.50 kcal mol^{-1}), tetramethylethylenediamine ($E^{(2)}$ = 88.47 kcal mol^{-1}) and anionic β-ketiminate ($E^{(2)}$ = 82.47 kcal mol^{-1}), with the contribution from π-backdonation overall comparable to that in complexes **4**-**6** ($E^{(2)}$ = 28.67-31.50 kcal mol^{-1}). At the same time, the complex with a tridentate N-donor ligand, hydrotris(3,5-dimethyl-1-pyrazolyl)borate features similar relative contributions from σ-donation ($E^{(2)}$ = 64.94 kcal mol^{-1}) and π-backdonation ($E^{(2)}$ = 30.59 kcal mol^{-1}) resembling the situation in complexes **4**-**6**. In all considered cases, the donation from σ-bonding C=C orbital to the Cu(*s*)-based orbital is very weak ($E^{(2)}$ = 1.60−2.99 kcal mol^{-1}).

NBO analysis of the binuclear complex **7** shows two interactions of the π(C=C)-type orbital to each of the two Cu-based *s*-type orbitals ($E^{(2)}$ = 28.34 kcal mol^{-1} for each interaction), showing that each of these two interactions is comparatively weaker than in the mononuclear analogue **4** ($E^{(2)}$ = 67.18 kcal mol^{-1}). The backdonation from each of the Cu-based $d_{x^2-y^2}$-type orbital to ethylene π*(C=C) orbital ($E^{(2)}$ = 28.53, 28.52 kcal mol-1) is also present, comparable to that in complexes **4**-**6** ($E^{(2)}$ = 27.74-29.90 kcal mol^{-1}) (Figure 4 and Table 4). Interestingly, complex **7** features increased contribution from the donation of the σ-C=C orbital to each Cu(*s*) ($E^{(2)}$ = 4.87 kcal mol^{-1} for each interaction), which is noticeably stronger than in mononuclear complexes **4**-**6** ($E^{(2)}$ = 0.85-1.17 kcal mol^{-1}).

Wiberg Bond Indices (WBI) corresponding to the ethylene C=C bond are summarized in Table 5. Consistent with the above analysis and the observed trend in C=C bond distances obtained in the X-ray structures, the WBI changes in the following order: free ethylene > **4** ≈ **5** > **6** > **7**.

Table 4. Key interactions between ethylene and copper in complexes **4**-**7**.

Donor (orbital #)	Acceptor (orbital #)	$E^{(2)}$, kcal mol^{-1}
*Complex **4***		
π(C=C) (#76)	Cu(*s*) (#82)	67.18
Cu($d_{x^2-y^2}$) (#29)	π*(C=C) (#125)	27.82
σ(C=C) (#75)	Cu(*s*) (#82)	1.06
*Complex **5***		
π(C=C) (#44)	Cu(*s*) (#90)	67.40
Cu($d_{x^2-y^2}$) (#31)	π*(C=C) (#99)	27.74
σ(C=C) (#43)	Cu(*s*) (#90)	1.17
*Complex **6***		
π(C=C) (#51)	Cu(*s*) (#114)	71.92
Cu($d_{x^2-y^2}$) (#37)	π*(C=C) (#124)	29.90
σ(C=C) (#50)	Cu(*s*) (#114)	0.85
*Complex **7***		
Cu($d_{x^2-y^2}$) (#51)	π*(C=C) (#169)	28.53
Cu($d_{x^2-y^2}$) (#60)	π*(C=C) (#169)	28.52
π(C=C) (#77)	Cu(*s*) (#155)	28.34
π(C=C) (#77)	Cu(*s*) (#156)	28.34
σ(C=C) (#76)	Cu(*s*) (#155)	4.87
σ(C=C) (#76)	Cu(*s*) (#156)	4.87

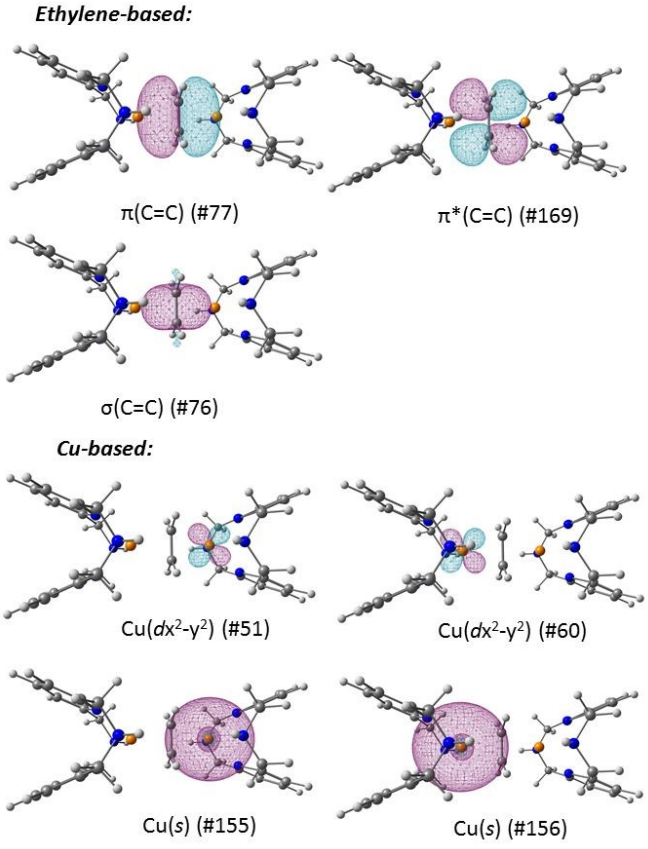

Figure 4. Selected natural bond orbital plots for complex **7**. Orbital numbers and types correspond to those in Table 4.

View Article Online
DOI: 10.1039/D2DT02180G

Table 5. Wiberg Bond Indices (WBI) corresponding to a C=C bond in free ethylene and DFT-optimized cationic parts of complexes **4**-**7**.

Ethylene	**4**	**5**	**6**	**7**
2.04	1.64	1.64	1.61	1.42

The QTAIM analysis of DFT-optimized structures located the presence of the bond critical points (bcp's) between Cu and carbon atoms of the ethylene in all complexes, as well as the ring critical point (rcp) corresponding to the Cu–C–C cycle. The bcp's are also present between the Cu atom and each of the four nitrogen atoms of the pyridinophane ligand in all complexes. The selected topological parameters at the bcp corresponding to the C=C ethylene bond are given in Table 6 (see the ESI for more detail). The value of the electron density at the bcp, indicative of a bond strength, decreases in the order: ethylene > **4** ≈ **5** > **6** > **7**. The delocalization index (an average number of electrons shared between a pair of atoms) also decreases in the same order, correlating with the trend in C=C bond lengths obtained from X-ray crystal structures. In turn, the value of the Laplacian of electron density at the saddle point (3, –1) is negative, but increases, which indicates the electron density deconcentration of the covalent C=C bond in the indicated series. The bond paths connecting the Cu atom and ethylene carbon are slightly curved inward in the proximity of carbon atoms, which has previously been reported as a common feature of transition metal olefin complexes, showing both σ-donation and a back-donation into a π*-orbital according to the DCD model (Figure 5 for complex **7** and Figures S61-S63 in the ESI for complexes **4**-**6**).[51-53]

Table 6. Electron density (ρ_b; in a.u.) and its Laplacian ($\nabla^2\rho_b$; in a.u.) at bcp and delocalization index (DI) corresponding to the C=C bond in the DFT-optimized cationic parts of complexes **4**-**7**.

Parameter:	Ethylene	**4**	**5**	**6**	**7**
ρ_b	0.342	0.308	0.308	0.305	0.273
$\nabla^2\rho_b$	–0.979	–0.793	–0.792	–0.771	–0.592
DI	1.896	1.443	1.442	1.410	1.207

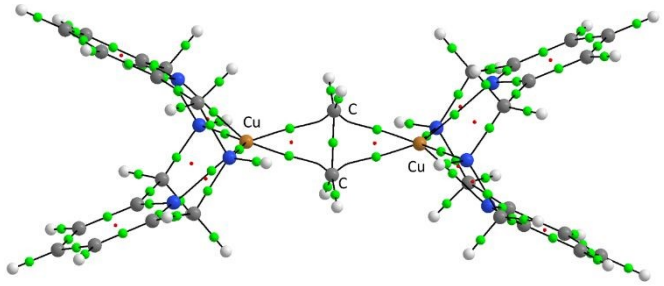

Figure 5. Molecular graph for "gas-phase" DFT-optimized cationic part of complex **7**. Bond critical points (3, –1) with a threshold of electron density above 0.025 a.u. and corresponding bond paths are shown with green dots and black lines, respectively. Ring critical points (3, +1) are shown as red dots.

The Laplacian of electron density $\nabla^2\rho(\boldsymbol{r})$ describes the curvature of electron density and thus points to regions of electron density concentration ($\nabla^2\rho(\boldsymbol{r}) < 0$) and depletion ($\nabla^2\rho(\boldsymbol{r}) > 0$). Figure 6 shows the distribution of this function for η^2-mono and μ-η^2-η^2-di nuclear complexes **4** and **7** with the same ^{H}N4 ligand. In the map planes, the copper atom features four lobes of valence shell charge concentration (VSCC) contracted to the nucleus and a wide deconcentration region, which that envelopes the metal center from the ligands so that the bcp's turn out to be depleted. The coordination bonds considered demonstrate a donor–acceptor mechanism of formation since the VSCC of N_{py}-atoms corresponding to the electron pair and the VSCC of ethylene carbon atoms attributed to the π-component appeared to be directed into internodes between the abovementioned lobes of Cu atom. In the case of N_{py}–Cu bonds, the bond path crosses N_{py}-atom's lobe and Cu-atom's internode, while C–Cu bond path tends to pass through more concentrated regions, which leads to its curve trajectory, especially for the gradient line between the carbon atom and bcp. Further, a comparison of the maps for complexes **4** and **7** makes it possible not only to reveal the asymmetry and symmetry of the electron density curvature above and below the ethylene ligand, respectively, but also significant deconcentration in the internuclear region on the C=C bond in the case of binuclear Cu complex **7** (see also Table 6).

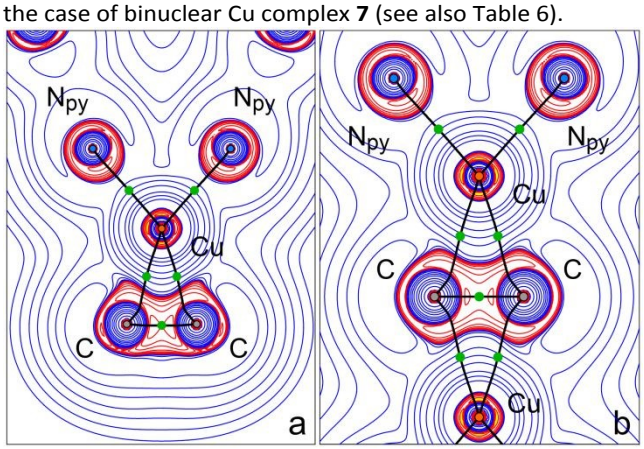

Figure 6. Contour maps of the distribution of the Laplacian of electron density $\nabla^2\rho(\boldsymbol{r})$ for "gas-phase" DFT-optimized cationic parts of **4** (a) and **7** (b) in the planes of labelled atoms. A logarithmic scale is adopted; blue and red colours correspond to positive and negative function values, respectively. Valence shell charge concentration lobes of copper atoms are highlighted in yellow. Critical points (3, –1) and bond paths are shown as green circles and black lines.

Overall, this analysis shows that ethylene coordination to two Cu atoms leads to much more significant weakening of the C=C bond as compared to the mononuclear analogues, likely due to the presence of π-back-donation from both copper atoms. The interesting feature of complex **7** is its also apparently larger donor contribution from the σ(C=C) orbital to the metal when compared to the mononuclear complexes **4**-**6**, although it remains weaker when compared to the classical mode of ethylene binding described by the DCD model.[49]

Conclusions

In summary, we report the reactivity of ethylene with copper(I) complexes supported by the tetradentate pyridinophane ligand (^{R}N4). In all cases, ethylene binds to the Cu center replacing MeCN. In the case of less sterically demanding ^{H}N4 and ^{Me}N4 ligands, ethylene effectively competes with MeCN binding even in the presence of excess MeCN, while the more hindered

View Article Online
DOI: 10.1039/D1DT02480C

(^{tBu}N4)Cu^{I} complex readily undergoes ethylene loss in the presence of MeCN. In all cases, ethylene binding leads to a significant shift of the anodic peak potential towards more positive values, as compared to the acetonitrile-bound complexes. Interestingly, formation of a binuclear complex is observed in the case of the least bulky (^{H}N4)Cu^{I} complex, featuring an unusual bridging mode of ethylene coordination between two Cu atoms, which leads to significant elongation of the C=C bond in coordinated ethylene, presumably due to π-back-donation from two copper atoms.

Experimental

General specifications

[^{R}N4Cu^{I}(MeCN)]PF_6 (**1**-**3**) were prepared in accordance with the reported procedure by reacting each ^{R}N4 ligands with same equivalent of tetrakis(acetonitrile)copper(I) hexafluorophosphate, followed by crystallization with acetonitrile–diethyl ether multiple times.[26] The procedures for the ligand synthesis are given in the ESI.

NMR spectra were measured on JEOL ECZ600R or JEOL ECZ400S NMR spectrometers. The X-ray diffraction data for the single crystals **4**-**7** were collected on a Rigaku XtaLab PRO diffractometer. Electrospray Ionization Mass Spectrometry (ESI-MS) measurements were performed on a Thermo Scientific ETD apparatus. Elemental analyses were performed using an Exeter Analytical CE440 instrument. FT-IR spectra were measured using an Agilent Cary 630 with an ATR module in an argon-filled glovebox. UV/vis absorption spectra were collected using an Agilent Cary 60 instrument. Cyclic voltammetry was performed using ALS/CHI electrochemical analyzers 660E. Pt disk electrode (d = 1.6 mm) as the working electrode, a platinum wire as the auxiliary electrode, and non-aqueous silver wire reference electrode assembly filled with a 0.01 M $AgNO_3$/0.1 M $^{n}Bu_4NClO_4$/MeCN solution were used. Photoluminescence spectra and photoluminescence quantum yields were recorded using a Hamamatsu Quantaurus-QY Plus spectrometer (excitation wavelength is 350 nm). A solid sample placed on a quartz dish was purged with nitrogen gas for 30 min in the integration sphere and measured keeping nitrogen gas flow.

Synthesis of 4

Method A. In a glove box, **1** (70.6 mg, 0.144 mmol) and anhydrous acetone (2 mL) were placed in a Schlenk tube. The tube was taken out of the glove box. The cap of the Schlenk tube was opened under Ar gas flow, then ethylene gas was bubbled to the solution through a needle for 30 seconds. A solution of anhydrous acetone–diethyl ether (1:1/v:v) (4 mL), then anhydrous diethyl ether (15 mL), which were prepared in the glove box, were placed over the acetone solution slowly to make two layers in the tube while keeping ethylene gas flow. After the tube was capped, the mixture was left for 2 days to diffuse slowly to provide crystals of the target product. After removing supernatant using a pipette under Ar gas flow, the obtained solid was dried under vacuum. The tube was filled with Ar gas, then brought into a glove box and the yellowish crystalline solid was collected (64.8 mg, 94%).

Method B. In a glovebox, **1** (23.4 mg, 0.0463 mmol) was dissolved in 15 mL of acetone in a round bottom Schlenk flask equipped with a stir bar. The Schlenk flask was sealed with a septum and taken outside of glove box. First, the Ar atmosphere inside the flask was removed under vacuum, then ethylene gas was introduced, which turned the solution from orange to pale yellow immediately. The solvent was evaporated under reduced pressure, while keeping a small ethylene flow. The obtained pale yellow powder was dried further under vacuum and then introduced inside the glove box. The product was dissolved in a minimum amount of acetone and set for recrystallization by vapor diffusion with pentane to give yellow crystals of **4** (11.3 mg, 53%).

^{1}H NMR (400 MHz, acetone-d_6): 7.59 (t, $^3J_{HH}$ = 6.6 Hz, p-***H***$_{Py}$, 2H), 7.10 (d, $^3J_{HH}$ = 6.9 Hz, m-***H***$_{Py}$, 4H), 4.63 (d, $^2J_{HH}$ = 16 Hz, 4H, Py-C***H***$_2$-N), 4.32 (s, 4H, ethylene), 4.14 (br, 2H, N-***H***), 3.93 (d, $^2J_{HH}$ = 16 Hz, 4H, Py-C***H***$_2$-N). ^{13}C NMR (100 MHz, acetone-d_6): 158.9 (o-***C***$_{Py}$), 138.7 (p-***C***$_{Py}$), 122.8 (m-***C***$_{Py}$), 76.8 (ethylene), 55.8 (Py-***C***H$_2$-N). ^{19}F NMR (376 MHz, acetone-d_6): −72.5 (d, $J_{P,F}$ = 708 MHz).

ESI-HRMS m/z calcd for $[C_{14}H_{16}N_4Cu]^+$ (−C_2H_4) = 303.0671, found: 303.0667. FT-IR (ATR, solid): 744 (m), 798 (m), 833 (s), 1002 (w), 1089 (w), 1123 (w), 1161 (w), 1221 (w), 1319 (w), 1437 (w), 1465 (w), 1580 (m), 1601 (w), 1715 (w), 2857 (br), 3380 (w). Elemental analysis. Found (calcd for $C_{16}H_{20}N_4CuPF_6$) C, 39.61 (40.30), H, 3.94 (4.23), N, 11.72 (11.75)

Synthesis of 5

The same procedure as method A described above for synthesis of **4** was used. A complex **2** (30.4 mg, 0.0587 mmol) solution in anhydrous acetone (2 mL) was reacted with ethylene to give the target product **5** as yellowish, crystalline solid (25.1 mg, yield 85%).

^{1}H NMR (400 MHz, acetone-d_6): 7.58 (t, $^3J_{HH}$ = 7.8 Hz, p-***H***$_{Py}$, 2H), 7.05 (d, $^3J_{HH}$ = 7.8 Hz, m-***H***$_{Py}$, 4H), 4.44 (s, 4H, ethylene), 4.33 (d, $^2J_{HH}$ =16 Hz, 4H, Py-C***H***$_2$-N), 3.83 (d, $^2J_{HH}$ = 16 Hz, 4H, Py-C***H***$_2$-N), 2.96 (s, 6H, N-C***H***$_3$). ^{13}C NMR (100 MHz, acetone-d_6): 157.9 (o-***C***$_{Py}$), 139.4 (p-***C***$_{Py}$), 123.3 (m-***C***$_{Py}$), 77.1 (ethylene), 64.5 (Py-***C***H$_2$-N), 47.6 (-***C***H$_3$). ^{19}F NMR (376 MHz, acetone-d_6): −72.5 (d, $J_{P,F}$ = 708 MHz). ESI-HRMS m/z calcd for $[C_{16}H_{20}\ N_4Cu]^+$ (−C_2H_4) = 331.0984, found : 331.0981. FT-IR (ATR, solid): 759 (w), 805 (s), 833 (s), 872 (w), 977 (w), 1011 (w), 1030 (w), 1091 (w), 1127 (w), 1162 (w), 1213 (w), 1228 (w), 1375 (w), 1448 (m), 1467 (w), 1574 (m), 1598 (w). Elemental analysis. Found (calcd for $C_{18}H_{24}N_4CuPF_6$) C, 42.62 (42.82), H, 4.49 (4.79), N, 10.80 (11.10)

Synthesis of 6

The same procedure as method A described above for synthesis of **4** was used. A complex **3** (30.7 mg, 0.0510 mmol) solution in anhydrous acetone (3 mL) was reacted with ethylene to give needle shaped, yellowish crystals of **6** (24.8 mg, yield 83%).

^{1}H NMR (400 MHz, acetone-d_6): 7.82 (t, $^3J_{HH}$ = 7.09 Hz, p-***H***$_{Py}$, 2H), 7.37 (d, $^3J_{HH}$ = 7.09 Hz, m-***H***$_{Py}$, 4H), 4.63 (d, $^2J_{HH}$ = 16 Hz, 4H, Py-C***H***$_2$-N), 4.16 (s, 4H, ethylene), 3.54 (d, $^2J_{HH}$ = 16 Hz, 4H, Py-C***H***$_2$-N), 1.37 (s, 18H, CC***H***$_3$). ^{13}C NMR (100MHz, acetone-d_6): 160.6 (o-***C***$_{Py}$), 140.2 (p-***C***$_{Py}$), 123.1 (m-***C***$_{Py}$), 75.5 (ethylene), 58.9 (***C***(CH$_3$)$_3$), 55.2 (Py-***C***H$_2$-N), 26.4 (C(***C***H$_3$)$_3$). ^{19}F NMR (376 MHz, acetone-d_6): −72.5 (d, $J_{P,F}$ = 705 MHz). ESI-HRMS m/z calcd for $[C_{22}H_{32}N_4Cu]^+$ (−C_2H_4) = 415.1923, found: 415.1910. FT-IR (ATR, solid): 709 (w), 771 (w), 789 (m), 833 (s), 878 (w), 919 (w), 991

(w), 1023 (w), 1057 (w), 1091 (w), 1124 (w), 1194 (m), 1225 (w), 1246 (w), 1262 (w), 1299 (w), 1368 (w), 1376 (w), 1400 (w), 1433 (w), 1459 (w), 1479 (w), 1520 (w), 1571 (w), 1597 (w). Elemental analysis. Found (calcd for $C_{24}H_{36}N_4CuPF_6$) C, 49.19 (48.93), H, 6.09 (6.16), N, 9.45 (9.51)

Synthesis of 7

In a glove box, complex **1** (5.0 mg, 10.2 μmol) was added to anhydrous acetone (5 mL) in a 20 mL vial and stirred at room temperature until complete dissolution, then **4** (5.0 mg, 10.5 μmol) was added, and stirring was stopped after addition. The vial was placed inside a bigger, capped glass vial containing pentane (ca. 10 mL) for vapour diffusion of pentane into the acetone solution under a N_2 atmosphere. After 3 days, yellow crystal formed on the bottom of the vial were collected, washed with pentane, and dried under vacuum to give yellow crystals of **7** (6.7 mg, yield 69%). The structure of **7** was confirmed by SC-XRD. Complex **7** is not soluble in non-polar solvents and its dissolution in acetone or MeCN gives rise to a set of broadened signals and insoluble precipitate, among which complex **4** could be identified by the presence of a characteristic peak at 4.32 ppm (coordinated ethylene).

FT-IR (ATR, solid): 741 (m), 829 (m), 1003 (w), 1089 (w), 1124 (w), 1162 (w), 1248 (w), 1319 (w), 1358 (w), 1436 (w), 1466 (w), 1580 (m), 1601 (w), 1715 (w), 1601 (w), 1715 (w), 2858 (br), 3385 (w).

Conflicts of interest

There are no conflicts to declare.

Acknowledgements

We thank Dr. Olga Gladkovskaya for the synthesis of ligand precursor. We also thank OIST Engineering section and Instrumental Analysis section at OIST for technical support, especially Dr. Hyung Been Kang (MEMS, OIST) and Dr. Michael Roy (IAS, OIST). R. R. F. acknowledges the support of RSF (grant No. 21-73-10191) in the part of crystal structure determination and topological analysis. We thank Dr. Shrinwantu Pal for helpful discussions regarding NBO analysis.

Notes and references

1. J. R. Ecker, *Science*, 1995, **268**, 667-675.
2. R. F. Lacey and B. M. Binder, *J. Inorg. Biochem.*, 2014, **133**, 58-62.
3. J. S. Thompson, R. L. Harlow and J. F. Whitney, *J. Am. Chem. Soc.*, 1983, **105**, 3522-3527.
4. H. Masuda, N. Yamamoto, T. Taga, K. Machida, S. Kitagawa and M. Munakata, *J. Organomet. Chem.*, 1987, **322**, 121-129.
5. J. Dai, M. Yamamoto, T. Kuroda-Sowa, M. Maekawa, Y. Suenaga and M. Munakata, *Inorg. Chem.*, 1997, **36**, 2688-2690.
6. B. F. Straub, F. Eisenträger and P. Hofmann, *Chem. Commun.*, 1999, 2507-2508.
7. X. Dai and T. H. Warren, *Chem. Commun.*, 2001, 1998-1999.
8. H. V. R. Dias, H.-L. Lu, H.-J. Kim, S. A. Polach, T. K. H. H. Goh, R. G. Browning and C. J. Lovely, *Organometallics*, 2002, **21**, 1466-1473.
9. R. M. Sullivan, H. Liu, D. S. Smith, J. C. Hanson, D. Osterhout, M. Ciraolo, C. P. Grey and J. D. Martin, *J. Am. Chem. Soc.*, 2003, **125**, 11065-11079.
10. H. V. R. Dias, X. Wang and H. V. K. Diyabalanage, *Inorg. Chem.*, 2005, **44**, 7322-7324.
11. G. Santiso-Quiñones, A. Reisinger, J. Slattery and I. Krossing, *Chem. Commun.*, 2007, 5046-5048.
12. H. V. R. Dias and J. Wu, *Eur. J. Inorg. Chem.*, 2008, 509-522.
13. J. A. Flores and H. V. R. Dias, *Inorg. Chem.*, 2008, **47**, 4448-4450.
14. J. J. Allen and A. R. Barron, *Dalton Trans.*, 2009, 878-890.
15. V. A. K. Adiraju, J. A. Flores, M. Yousufuddin and H. V. R. Dias, *Organometallics*, 2012, **31**, 7926-7932.
16. H. V. R. Dias and J. Wu, *Organometallics*, 2012, **31**, 1511-1517.
17. P. Ebrahimpour, M. F. Haddow and D. F. Wass, *Inorg. Chem.*, 2013, **52**, 3765-3771.
18. M. Fianchini, C. F. Campana, B. Chilukuri, T. R. Cundari, V. Petricek and H. V. R. Dias, *Organometallics*, 2013, **32**, 3034-3041.
19. K. Klimovica, K. Kirschbaum and O. Daugulis, *Organometallics*, 2016, **35**, 2938-2943.
20. S. G. Ridlen, J. Wu, N. V. Kulkarni and H. V. R. Dias, *Eur. J. Inorg. Chem.*, 2016, **2016**, 2573-2580.
21. B. Esser, J. M. Schnorr and T. M. Swager, *Angew. Chem. Int. Ed.*, 2012, **51**, 5752-5756.
22. B. Esser and T. M. Swager, *Angew. Chem. Int. Ed.*, 2010, **49**, 8872-8875.
23. W. Fu, T. F. van Dijkman, L. M. C. Lima, F. Jiang, G. F. Schneider and E. Bouwman, *Nano Lett.*, 2017, **17**, 7980-7988.
24. D. Parasar, A. H. Elashkar, A. A. Yakovenko, N. B. Jayaratna, B. L. Edwards, S. G. Telfer, H. V. R. Dias and M. G. Cowan, *Angew. Chem. Int. Ed.*, 2020, **59**, 21001-21006.
25. G. A. Filonenko, R. R. Fayzullin and J. R. Khusnutdinova, *J. Mater. Chem. C*, 2017, **5**, 1638-1645.
26. P. H. Patil, G. A. Filonenko, S. Lapointe, R. R. Fayzullin and J. R. Khusnutdinova, *Inorg. Chem.*, 2018, **57**, 10009-10027.
27. A. Karimata, P. H. Patil, E. Khaskin, S. Lapointe, R. R. Fayzullin, P. Stampoulis and J. R. Khusnutdinova, *Chem. Commun.*, 2020, **56**, 50-53.
28. A. Karimata, P. H. Patil, R. R. Fayzullin, E. Khaskin, S. Lapointe and J. R. Khusnutdinova, *Chem. Sci.*, 2020, **11**, 10814-10820.
29. Deposition Numbers CCDC 2176964 (**4**), 2176965 (**5**), 2176966 (**6**), and 2176967 (**7**) contain the supplementary crystallographic data for this paper. These data are provided free of charge by the joint Cambridge Crystallographic Data Centre and Fachinformationszentrum Karlsruhe Access Structures service www.ccdc.cam.ac.uk/structures.
30. G. J. H. Nes and A. Vos, *Acta. Crystallogr. B.*, 1979, **35**, 2593-2601.
31. M. J. Bainbridge, J. R. L. Smith and P. H. Walton, *Dalton Trans.*, 2009, 3143-3152.
32. S. M. Nelson, A. Lavery and M. G. B. Drew, *J. Chem. Soc., Dalton Trans.*, 1986, 911-920.
33. M. Håkansson, C. Lopes and S. Jagner, *Organometallics*, 1998, **17**, 210-215.

View Article Online
DOI: 10.1039/D2DT02180C

34. M. Håkansson, K. Brantin and S. Jagner, *J. Organomet. Chem.*, 2000, **602**, 5-14.
35. B. F. Straub, I. Gruber, F. Rominger and P. Hofmann, *J. Organomet. Chem.*, 2003, **684**, 124-143.
36. A. T. Royappa, A. D. Royappa, R. F. Moral, A. L. Rheingold, R. J. Papoular, D. M. Blum, T. Q. Duong, J. R. Stepherson, O. D. Vu, B. Chen, M. R. Suchomel, J. A. Golen, G. André, N. Kourkoumelis, A. D. Mercer, A. M. Pekarek and D. C. Kelly, *Polyhedron*, 2016, **119**, 563-574.
37. F. A. Cotton and P. A. Kibala, *Polyhedron*, 1987, **6**, 645-646.
38. F. A. Cotton and P. A. Kibala, *Inorg. Chem.*, 1990, **29**, 3192-3196.
39. T. Takahashi, K. Kasai, N. Suzuki, K. Nakajima and E. Negishi, *Organometallics*, 1994, **13**, 3413-3414.
40. F. J. Fernández, P. Gómez-Sal, A. Manzanero, P. Royo, H. Jacobsen and H. Berke, *Organometallics*, 1997, **16**, 1553-1561.
41. R. Fischer, D. Walther, P. Gebhardt and H. Görls, *Organometallics*, 2000, **19**, 2532-2540.
42. P. J. Shapiro, W. P. Schaefer, J. A. Labinger, J. E. Bercaw and W. D. Cotter, *J. Am. Chem. Soc.*, 1994, **116**, 4623-4640.
43. C. J. Burns and R. A. Andersen, *J. Am. Chem. Soc.*, 1987, **109**, 915-917.
44. W. H. Monillas, G. P. A. Yap, L. A. MacAdams and K. H. Theopold, *J. Am. Chem. Soc.*, 2007, **129**, 8090-8091.
45. F. A. Cotton, E. V. Dikarev, M. A. Petrukhina and R. E. Taylor, *J. Am. Chem. Soc.*, 2001, **123**, 5831-5832.
46. T. Ziegler and A. Rauk, *Inorg. Chem.*, 1979, **18**, 1558-1565.
47. J. Chatt, L. A. Duncanson and L. M. Venanzi, *J. Chem. Soc.*, 1955, 4456-4460.
48. J. Chatt and L. A. Duncanson, *J. Chem. Soc.*, 1953, 2939-2947.
49. C. P. Gordon, R. A. Andersen and C. Copéret, *Helv. Chim. Acta*, 2019, **102**, e1900151.
50. R. F. W. Bader, *Chem. Rev.*, 1991, **91**, 893-928.
51. N. Hebben, H.-J. Himmel, G. Eickerling, C. Herrmann, M. Reiher, V. Herz, M. Presnitz and W. Scherer, *Chem. Eur. J.*, 2007, **13**, 10078-10087.
52. P. Macchi, D. M. Proserpio and A. Sironi, *J. Am. Chem. Soc.*, 1998, **120**, 1447-1455.
53. R. H. Hertwig, W. Koch, D. Schröder, H. Schwarz, J. Hrušák and P. Schwerdtfeger, *J. Phys. Chem.*, 1996, **100**, 12253-12260.